



## In Situ Determination of the Nanoscale Chemistry and Behavior of Solid-Liquid Systems

Santhana K. Eswaramoorthy, *et al.*

*Science* **318**, 1437 (2007);

DOI: 10.1126/science.1146511

**The following resources related to this article are available online at [www.sciencemag.org](http://www.sciencemag.org) (this information is current as of December 7, 2007):**

**Updated information and services**, including high-resolution figures, can be found in the online version of this article at:

<http://www.sciencemag.org/cgi/content/full/318/5855/1437>

**Supporting Online Material** can be found at:

<http://www.sciencemag.org/cgi/content/full/318/5855/1437/DC1>

This article **cites 22 articles**, 4 of which can be accessed for free:

<http://www.sciencemag.org/cgi/content/full/318/5855/1437#otherarticles>

This article appears in the following **subject collections**:

Materials Science

[http://www.sciencemag.org/cgi/collection/mat\\_sci](http://www.sciencemag.org/cgi/collection/mat_sci)

Information about obtaining **reprints** of this article or about obtaining **permission to reproduce this article** in whole or in part can be found at:

<http://www.sciencemag.org/about/permissions.dtl>

# In Situ Determination of the Nanoscale Chemistry and Behavior of Solid-Liquid Systems

Santhana K. Eswaramoorthy,<sup>1</sup> James M. Howe,<sup>1\*</sup> Govindarajan Muralidharan<sup>2</sup>

Many fundamental questions in crystal-growth behavior remain unanswered because of the difficulties encountered in simultaneously observing phases and determining elemental concentrations and redistributions while crystals nucleate and grow at the nanoscale. We show that these obstacles can be overcome by performing energy-dispersive x-ray spectroscopy on partially molten Al-Si-Cu-Mg alloy particles during in situ heating in a transmission electron microscope. Using this technique, we were able to (i) determine that the aluminum and silicon concentrations change in a complementary and symmetric manner about the solid-liquid interface as a function of temperature; (ii) directly measure the solid- and liquid-phase compositions at equilibrium and in highly undercooled conditions for quantitative comparison with thermodynamic calculations of the liquidus and solidus phase boundaries; and (iii) provide direct evidence for homogeneous nucleation of the aluminum-rich solid.

Crystal growth is an important technological process affecting fields from metallurgy to solid-state physics and applications ranging from the production of metal-alloy ingots for buildings and aircraft to single-crystal semiconductors and oxides for electronic and optical devices (1, 2). It is also involved in everyday natural phenomena such as the freezing of water, and biomineralization of living organisms (3), and in geological processes such as the formation of stalactites and stalagmites in caves (4). Understanding fundamental phenomena such as the structure and composition of the solid-liquid interface, the partitioning of elements between the solid and liquid phases during crystal growth, and critical factors involved in the nucleation of phases is essential to solidification science and the development of new material structures under equilibrium and nonequilibrium conditions (1, 5–7). The challenges of directly determining these features have been largely beyond the capabilities of experimentalists (8), although recent progress has been made in determining the atomic structure of the solid-liquid interface (9–11). This problem is particularly severe in inorganic engineering materials, which usually have high melting points (typically greater than 800 K) and are optically opaque.

Tumbull and Cech (12) showed that heterogeneous nucleation on impurities could be eliminated during the freezing of metals and semi-metals by using liquid droplets a few tens of micrometers in diameter. Since then, investigators have found that solidification of alloy droplets under conditions far from equilibrium has the potential to produce metastable phases with novel properties and to broaden the study of solidification processes (7, 13). Al-

based alloys have received attention as model systems because it is possible to produce large undercoolings in atomized liquid droplets less than 20  $\mu\text{m}$  in diameter (7). In these studies, the aforementioned difficulties have precluded direct observation of the nucleation and growth behavior

of phases, or measurements of the local compositions present during solidification (or melting). The closest experiments of this type have involved in situ heating of submicrometer-diameter binary Al-Si alloy particles to obtain qualitative elemental profiles across solid-liquid interfaces (14, 15) in the transmission electron microscope (TEM). In this study, we used a newly designed thermal shield on a conventional TEM heating holder (16) to obtain quantitative chemical compositions across a solid-liquid interface and in the undercooled liquid phase as a function of temperature.

The sample chosen for this investigation was a multicomponent commercial, Al-Si base alloy (AA 390) powder obtained from Valimet (17). The alloy is typically used in aerospace and automobile applications because of its high strength-to-weight ratio and good wear and corrosion resistance. The alloy is mainly Al, with intentional additions of 17.87 Si, 1.83 Cu, and 0.6 Mg (here and henceforth, all compositions are in atomic percent). Additional minor impurities in the alloy such as Fe and Mn are generally present at lower amounts and are not relevant to the present study. The powder particles were suspended in ethanol and dispersed on an ultrathin

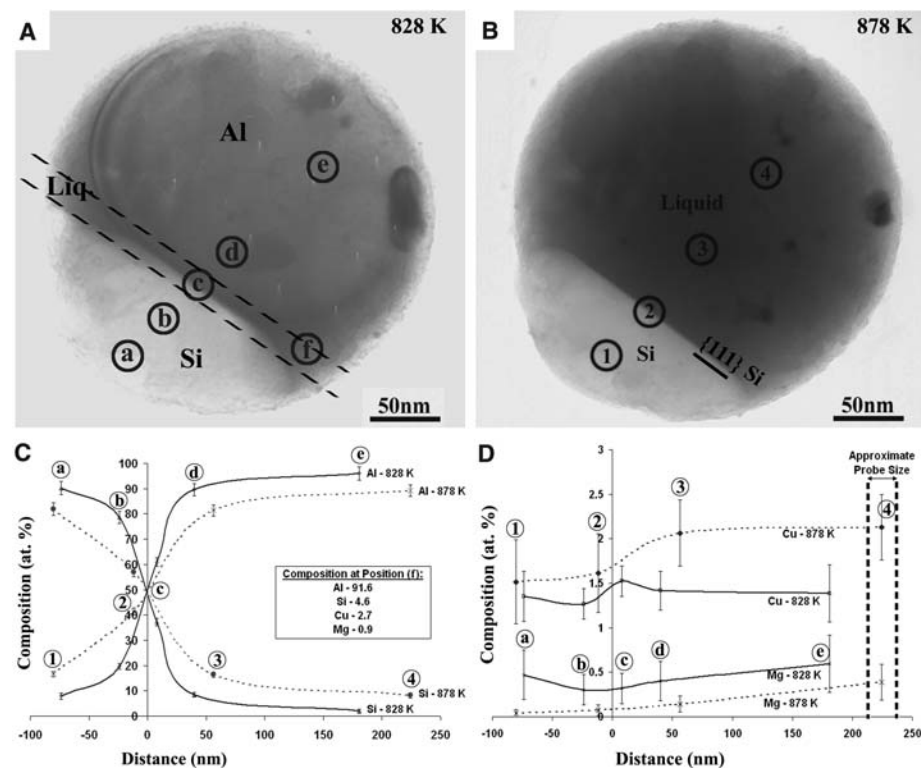


**Fig. 1.** (A) Bright-field TEM image of a partially molten Al-Si-Cu-Mg powder particle taken at a temperature of 828 K. The faint, dashed line parallel to the interface indicates the approximate appearance of the column of material sampled by the electron beam normal to the plane of the figure. Circles a through f indicate where x-ray spectra were acquired. [Reprinted from (16) courtesy of the Microscopy Society of America and Cambridge University Press] (B) Bright-field TEM image of the same powder particle after further heating to 878 K. Circles 1 through 4 indicate where x-ray spectra were acquired. (C) Concentration profiles of Al and Si obtained from x-ray spectra taken at 828 K (solid lines) and at 878 K (dashed lines). (D) Concentration profiles of Cu and Mg obtained from x-ray spectra taken at 828 K (solid lines) and at 878 K (dashed lines).

<sup>1</sup>Department of Materials Science and Engineering, University of Virginia, 140 Chemistry Drive, Charlottesville, VA 22904-4745, USA. <sup>2</sup>Materials Science and Technology Division, Oak Ridge National Laboratory, 1 Bethel Valley Road, Oak Ridge, TN 37831-6132, USA.

\*To whom correspondence should be addressed. E-mail: jh9s@virginia.edu

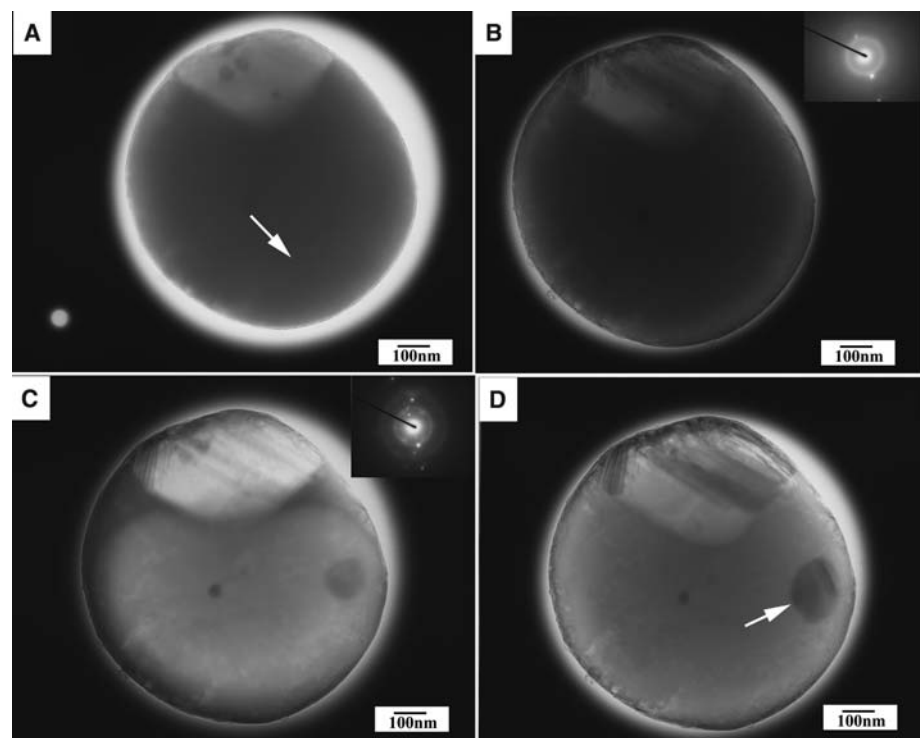
carbon film supported on a copper-mesh TEM grid. The in situ heating experiments were performed at 200 kV in a JEOL 2000FX-II TEM with a Gatan double-tilt heating holder. A thermocouple in the holder maintained the specimen temperature to within  $\pm 15$  K. Chemical compositions were determined by energy-dispersive x-ray spectroscopy (EDXS) with a Gresham high-angle x-ray detector and an incident electron beam diameter (probe size) of about 25 nm. Details regarding quantification of the x-ray spectra and the accuracy of the compositional measurements,

which are generally better than  $\pm 0.2\%$ , are provided in the Supporting Online Material.

Figure 1A shows a bright-field TEM image of an Al-Si-Cu-Mg powder particle about 350 nm in diameter, taken at a temperature of 828 K. The particle is partially molten, containing a faceted primary Si particle on the lower left and an oval-shaped solid Al-rich particle that is surrounded by Al-rich liquid phase in the upper right. An amorphous aluminum oxide film several nanometers thick forms naturally on the particle surface, and this oxide shell prevents the liquid phase

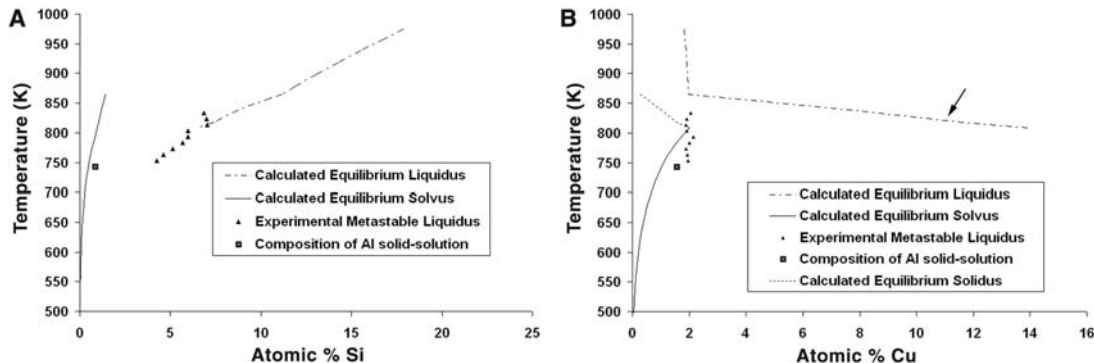
from evaporating in the TEM vacuum (18). The thin oxide is highly transparent and barely visible in the TEM images. The coexistence of two solid phases and a liquid in equilibrium at 828 K is consistent with Gibb's phase rule (19), because there are four major elements (Al, Si, Cu, and Mg) in the alloy. X-ray spectra were obtained at five positions, indicated by circles a to e in Fig. 1A (the size of the circle represents the approximate probe size), and the resulting compositions are plotted in Fig. 1, C and D. One additional composition obtained in the liquid phase only, circle f in Fig. 1A, is also given in Fig. 1C. Several important features are evident from these figures. The composition on the right side of the particle, at position e, contains approximately 96.0 Al, 1.9 Si, 1.3 Cu, and 0.5 Mg, while that in the Si on the far left, at position a, is about 90.2 Si, 7.9 Al, 1.3 Cu, and 0.4 Mg, indicating that the Cu and Mg levels are similar in the two solid phases at this temperature. As the thin, liquid interface between the two solid phases is approached from either side, the Al and Si concentrations change in a complementary and symmetric manner. The Cu and Mg levels do not change appreciably, except at position c, where the Cu concentration increases slightly. This increase is likely due to prior partitioning of Cu during solidification, because the first liquid formed during heating in the TEM was the last Cu-enriched liquid to solidify in the particle.

Figure 1B shows the same particle after further heating to a temperature of 878 K. The particle contains only two phases, solid Si in the lower left and Al-rich liquid in the remaining volume. Similar to Fig. 1A, x-ray spectra were obtained at four positions indicated by circles 1 to 4, and the resulting compositions are plotted in Fig. 1, C and D. As at 828 K, the Al and Si concentrations change in a complementary and symmetric manner about the solid-liquid interface as it is approached from either side. The Al concentration in the liquid on the far right has decreased to about 89.2, while the levels of Cu and Si have increased to about 2.1 and 8.1, respectively, due to partial dissolution of the solid Si and increased solubility of the Cu in the liquid phase with temperature (20, 21). Also, the partially dissolved Si particle has become highly faceted along a low-energy  $\{111\}$  plane (determined by electron diffraction), indicated in Fig. 1B. In contrast to the behavior observed at 828 K,



**Fig. 2.** (A) Bright-field TEM image of a second particle at 833 K. An arrow points to the position of the electron probe in the liquid in the analysis, and the bright spot in the lower-left corner is an image of the actual probe used. (B) Image at 753 K with an inset electron diffraction pattern showing the diffuse ring pattern corresponding to the liquid phase, as well as Si reflections. (C) Image at 743 K with an inset electron diffraction pattern showing additional spots due to the formation of crystalline Al-rich phase. Faint rings in the diffraction pattern correspond to a small fraction of remaining liquid. (D) Image at 743 K taken with a lower electron beam brightness to eliminate beam heating. Arrow points to the  $\text{Al}_2\text{Cu}$  phase identified by EDXS. The electron beam is condensed to just illuminate the particle in all of the images, so that the remaining background appears dark. The contrast visible in the Si crystal is due to defects, which change their orientation and contrast slightly with temperature.

**Fig. 3.** (A) Si and (B) Cu concentrations in the undercooled liquid phase plotted as a function of temperature in pseudobinary phase diagrams along with the calculated equilibrium liquidus, solidus, and solvus lines for the elements.



the Cu and Mg concentrations both decrease in going from the Al-rich liquid phase to the solid Si phase at 878 K, reflecting the increased solubility in the Al-rich liquid.

Comparison of the results from the chemical analyses taken across the solid-liquid interface and in the liquid phase in the in situ TEM experiments with values obtained from thermodynamic calculations generally yielded good qualitative agreement but limited quantitative agreement. According to the calculations, the Si concentration in the liquid should increase with temperature because of the progressive dissolution of the solid Si into the liquid phase. This is in good agreement with observations from the in situ experiments. Quantitatively, the in situ results showed an increase in Si concentration from 4.6 to 8.1 when the sample was heated from 828 to 878 K, whereas the calculations yielded a change in Si concentration from 8.3 to 12.1 for the same temperatures. The experimental Cu and Mg concentrations also qualitatively followed the calculated predictions. For example, the calculations predicted a decrease in concentration from 8.8 to 1.9 in Cu and from 2.9 to 0.6 in Mg when the temperature was raised from 828 to 878 K. In comparison, the in situ experiments showed a decrease from 2.7 to 2.1 Cu and from 0.9 to 0.3 Mg. The composition of the Al solid-solution (Fig. 1, C and D) at 828 K measured in the in situ TEM experiment was 96.0 Al, 1.3 Cu, 0.5 Mg, and 1.9 Si. This is in reasonably good agreement with the calculated value of 97.3 Al, 1.0 Cu, 0.3 Mg, and 1.1 Si. The slightly higher levels of Cu, Mg, and Si in the experiment may be due to a thin layer of liquid phase between the Al and oxide at location e.

Thermodynamic calculations predict that the Si phase does not have any solid solubility for Al, Mg, or Cu at any temperature. However, experimentally, the composition of the silicon phase was 90.2 Si, 7.9 Al, 1.3 Cu, and 0.4 Mg at 828 K. This difference could be partly due to a thin layer of liquid phase that overlaps the solid Si crystal through the specimen thickness in projection, but this process cannot account for the entire difference, because with 7.9 Al, the concentrations of Cu and Mg would be about 1.0 and 0.1, respectively. Hence, the experimental results indicate that the Si phase does have some solubility for Cu and Mg (and perhaps Al) at elevated temperatures. In situ, high-temperature composition measurements in the TEM thus provide valuable information that would enable more accurate descriptors of the thermodynamics of phases and hence phase equilibria.

To investigate metastable phase equilibria, we heated the sample in situ in the TEM and determined the lowest temperature at which the liquid phase was in equilibrium with primary Si on melting. This temperature was found to be about 833 K, and the corresponding bright-field image is shown in Fig. 2A. The temperature was then decreased from 833 K in 10 K steps, and x-ray spectra were acquired from the liquid and Si phase at the same positions on the particle (indicated for the liquid by an arrow in Fig. 2A). This process was repeated until homogeneous nucleation of the Al solid-

solution phase was observed to occur at 743 K, representing a cumulative undercooling of about 90 K.

A bright-field image of the sample at 753 K, just before nucleation, is shown in Fig. 2B. The corresponding electron diffraction pattern for the particle inset in Fig. 2B reveals a diffuse ring pattern due to short-range order in the liquid phase, verifying that the sample is in an undercooled metastable state. The crystalline spots also seen in the pattern correspond to the primary Si crystal. Further cooling by 10 to 743 K was sufficient to nucleate the crystalline Al-rich phase, and the electron diffraction pattern inset in Fig. 2C displays additional crystalline spots corresponding to this Al phase. The electron diffraction pattern also has fainter rings due to the small fraction of remaining liquid. A small amount of liquid phase can still be observed in Fig. 2C because the focused electron beam heats the particle slightly (22). Upon decreasing the brightness of the beam to eliminate this heating, the remaining liquid solidified, and the fully solid particle is shown in Fig. 2D. A small crystal with dark contrast (arrow) can be seen in the Al phase, and this was determined to be the  $\text{Al}_2\text{Cu}$  phase by EDXS.

The nucleation and growth of the solid Al-rich phase occurred and reached a size of about 800 nm in less than 0.03 s, the minimum time step of the TV camera, which records at 30 frames per second. This result suggests that the interface velocity during growth was at least  $1.3 \times 10^{-5}$  m/s and potentially much faster, given that the temperature gradient during solidification was on the order of  $2.3 \times 10^7$  K/m. Faster recording devices and/or TEMs specially designed to achieve ultrafast time resolution (23) are needed to follow the movement of such solid-liquid interfaces under these high-driving force, highly undercooled conditions.

The Si and Cu concentrations in the undercooled liquid phase are plotted in Fig. 3 as a function of temperature in pseudobinary phase diagrams, along with the computed equilibrium liquidus, solidus, and solvus lines for the elements. The quaternary system is plotted as a pseudobinary phase diagram to facilitate comparison between the experimental metastable liquidus lines (i.e., phase boundaries) and the calculated equilibrium liquidus/solvus lines. The experimental data for Si in Fig. 3A show that the composition of the metastable liquid phase qualitatively follows an extrapolation of the equilibrium liquidus line although some quantitative differences occur. The Si concentration does not change during the first three temperature steps. This could be due to the highly faceted nature of portions of the Si-liquid interface seen in Fig. 2A, which require a two-dimensional nucleation and growth process (5, 6) to absorb Si from the liquid. Owing to the kinetic barrier associated with this growth mechanism, it is possible that the liquid composition remained constant until there was sufficient undercooling for two-dimensional nucleation to occur, thereby allowing the Si crystal to grow and absorb Si from the liquid phase with further undercooling. The

composition at the lowest-temperature data point for the solid Al-rich phase is also given in Fig. 3A and qualitatively agrees with the calculated equilibrium solvus. The Cu concentrations also follow a line that is parallel to an extension of the equilibrium liquidus line and are substantially less than the compositions of the liquid that would be in equilibrium with the Al-rich phase (arrow in Fig. 3B). This occurs because Cu remains incorporated in the undercooled liquid until nucleation of the Al-rich phase occurs. Once the Al-rich phase nucleates, Cu is rejected from the growing solid phase, and the Cu concentration in the liquid rapidly increases. In the Al-rich solid, it abruptly changes to within a few tenths of a percent of the calculated equilibrium Cu solvus line (lowest temperature data point in Fig. 3B).

In addition to compositional measurements at the nanoscale, the approach used here enables direct observations to be performed on the behavior of solid-liquid interfaces. For example, the presence of the liquid phase surrounding the solid Al phase in Figs. 1A and 2C indicates that it is energetically unfavorable for the Al-rich solid to form an interface with either the solid Si or the oxide shell [i.e., the contact angle (6, 19) is  $180^\circ$ ]. This provides direct evidence that neither of these phases could have acted as a catalyst in the nucleation of the Al-rich solid. This result is in contrast to the inference of Turnbull and Cech (12) and agrees with more recent findings of Das *et al.* (7). Further, the oval shape of the solid Al seen in Figs. 1A and 2C is due to its conformance to the cavity created by the solid Si and surrounding oxide shell, rather than its unconstrained equilibrium shape, which is a sphere. In contrast, the solid Si particle has an anisotropic solid-liquid interfacial energy, because it displays clear facets. These morphological observations agree with the predictions of Jackson's  $\alpha$ -parameter calculation (5, 6, 24), which yields  $\alpha$  values for Si and Al of 3.6 and 1.4, respectively (based on their molar entropies of melting of 29.8 and 11.4 J/K), indicating that Si should facet and Al should not. It also agrees with other, more sophisticated, calculations predicting the same behavior (25).

Analyses like those shown above can be performed on all Al-base alloys prepared in powder form, because the thin aluminum oxide shell contains the molten metal in the high vacuum of the TEM. Nonpowder forms can be examined by using special TEM specimen-preparation methods (26). Low-vapor pressure alloys containing elements such as In and Sn, or the recently studied Au-Ge alloys (27, 28), can also be observed in high vacuum. For other metals and materials that have a high vapor pressure and do not form a structurally stable oxide layer, some way of containing the liquid phase has to be realized. Special liquid-cell holders have been developed for the TEM (29, 30) and in combination with a heating and cooling capability may be able to accommodate these materials in the future. For materials with higher melting temperatures (e.g., greater than about 900 K), further improvements in the

temperature capability of the heating-holder/x-ray detector system are needed. The use of smaller, brighter electron beams in state-of-the-art TEMs (31) can provide chemical resolutions approaching atomic dimensions. Having such direct morphological information, combined with high-spatial resolution chemical analysis, illustrates the potential for solving many important questions in crystallization science. Examples include whether the fundamental assumption of local equilibrium at solid-liquid interfaces in thermodynamic and kinetic models is valid, whether solid-liquid interface compositions change with crystal orientation, and if segregation occurs at solid-liquid interfaces. Clarification of the formation mechanisms shown in recent studies of nanodroplets (27) and nanowire growth (28) may also be possible.

#### References and Notes

1. M. Rappaz, C. Beckermann, R. Trivedi, Eds., *Solidification Processes and Microstructures: A Symposium in Honor of Prof. W. Kurz* (The Minerals, Metals and Materials Society, Warrendale, PA, 2004).
2. K. Byrappa, T. Ohachi, Eds., *Crystal Growth Technology* (William Andrew, New York, 2003); available at [www.knovel.com/knovel2/Toc.jsp?BookID=751&VerticalID=0](http://www.knovel.com/knovel2/Toc.jsp?BookID=751&VerticalID=0).
3. M. Sarikaya, C. Tamerler, A. K.-Y. Jen, K. Schulten, F. Baneyx, *Nat. Mater.* **2**, 577 (2003).
4. W. Dreybrodt, *Boreas* **28**, 347 (1999).

5. M. C. Flemings, *Solidification Processing* (McGraw-Hill, New York, 1974).
6. W. A. Tiller, *The Science of Crystallization: Microscopic Interfacial Phenomena* (Cambridge Univ. Press, Cambridge, UK, 1991).
7. S. K. Das, J. H. Perepezko, R. I. Wu, G. Wilde, *Mater. Sci. Eng. A* **304-306**, 159 (2001).
8. E. Johnson, *Science* **296**, 477 (2002).
9. H. Reichert et al., *Nature* **408**, 839 (2000).
10. S. E. Donnelly et al., *Science* **296**, 507 (2002).
11. S. H. Oh, Y. Kauffmann, C. Scheu, W. D. Kaplan, M. Ruehle, *Science* **310**, 661 (2005).
12. D. Turnbull, R. E. Cech, *J. Appl. Phys.* **21**, 804 (1950).
13. R. P. Liu, D. M. Herlach, M. Vandyoussefi, A. L. Greer, *Metall. Mater. Trans.* **35A**, 607 (2004).
14. S. Arai, S. Tsukimoto, H. Miyai, H. Saka, *J. Electron Microsc. (Tokyo)* **48**, 317 (1999).
15. G. A. Storaska, K. T. Moore, J. M. Howe, *Philos. Mag. A* **84**, 2619 (2004).
16. S. K. Eswaramoorthy, J. M. Howe, F. Phillipp, *Microsc. Microanal.* **13**, 291 (2007).
17. Valimet, 431 East Sperry Road, Stockton, CA 95206, USA.
18. G. A. Storaska, J. M. Howe, *Mater. Sci. Eng. A* **368**, 183 (2004).
19. C. Lupis, in *Chemical Thermodynamics of Materials* (Elsevier Science, New York, 1983), pp. 169–344, 373–375, 437–502.
20. L. F. Mondolfo, in *Aluminum Alloys: Structure and Properties* (Butterworths, London, 1976), pp. 368–376, 513–515, 644–651.
21. F. N. Rhines, *Phase Diagrams in Metallurgy: Their Development and Application* (McGraw-Hill, New York, 1956), pp 5–6, 220–242.
22. T. Yokota, J. M. Howe, M. Murayama, *Phys. Rev. Lett.* **91**, 265504 (2003).
23. W. E. King et al., *J. Appl. Phys.* **97**, 111101 (2005).
24. K. A. Jackson, *Liquid Metals and Solidification* (American Society for Metals, Cleveland, 1958).
25. K. A. Jackson, *Interface Sci.* **10**, 159 (2002).
26. J. Chang, T. Sakai, H. Saka, *Philos. Mag. A* **85**, 247 (2005).
27. P. W. Sutter, E. A. Sutter, *Nat. Mater.* **6**, 363 (2007).
28. S. Kodambaka, J. Tersoff, M. C. Reuter, F. M. Ross, *Science* **316**, 729 (2007).
29. T. L. Daulton, B. L. Little, K. Lowe, J. Jones-Meehan, *J. Microbiol. Methods* **50**, 39 (2002).
30. M. J. Williamson, R. M. Tromp, P. M. Vereecken, R. Hull, F. M. Ross, *Nat. Mater.* **2**, 532 (2003).
31. S. J. Pennycook, M. Varela, C. J. D. Hetherington, A. I. Kirkland, *MRS Bull.* **31**, 36 (2006).
32. This research was supported by the NSF under grants DMR-9908855 and DMR-0554792. The part of this work done at Oak Ridge National Laboratory was supported by the Assistant Secretary for Energy Efficiency and Renewable Energy, Office of FreedomCAR and Vehicle Technologies, Automotive Propulsion Materials Program, U.S. Department of Energy, under contract DE-AC05-00OR22725 with the University of Texas–Battelle, LLC. Use of instrumentation in the Nanoscale Materials Characterization Facility at UVA for this research is gratefully acknowledged.

#### Supporting Online Material

[www.sciencemag.org/cgi/content/full/318/5855/1437/DC1](http://www.sciencemag.org/cgi/content/full/318/5855/1437/DC1)  
Materials and Methods  
SOM Text  
References

14 June 2007; accepted 11 October 2007  
10.1126/science.1146511

## Fluctuation Superconductivity in Mesoscopic Aluminum Rings

Nicholas C. Koshnick,<sup>1</sup> Hendrik Bluhm,<sup>1</sup> Martin E. Huber,<sup>2</sup> Kathryn A. Moler<sup>1\*</sup>

Fluctuations are important near phase transitions, where they can be difficult to describe quantitatively. Superconductivity in mesoscopic rings is particularly intriguing because the critical temperature is an oscillatory function of magnetic field. There is an exact theory for thermal fluctuations in one-dimensional superconducting rings, which are therefore expected to be an excellent model system. We measured the susceptibility of many rings, one ring at a time, by using a scanning superconducting quantum interference device that can isolate magnetic signals that are seven orders of magnitude smaller than applied flux. We find that the fluctuation theory describes the results and that a single parameter characterizes the ways in which the fluctuations are especially important at magnetic fields where the critical temperature is suppressed.

Superconductivity requires both electron pairing and the coalescence of the pairs into a macroscopic quantum state with long-range phase coherence, usually described as a single wave function. In restricted geometries, thermal energy allows contributions from multiple wave functions to dramatically change the behavior of the system (1–3). Experimental knowledge of such fluctuations in one dimension (1D) is largely derived from transport measurements (4), which require electrical contacts and an externally

applied current. We used a contactless technique to study fluctuation effects in isolated, quasi-1D rings in the temperature range where the circumference is comparable to the temperature-dependent Ginzburg-Landau (G-L) coherence length,  $\xi(T)$ .

With use of a scanning micro-superconducting quantum interference device (SQUID), we detected the current in many individual quasi-1D aluminum rings, paying particular attention to small currents near each ring's superconducting transition temperature,  $T_c$ . Such measurements have many advantages. In 1D, the current about a ring,  $I$ , is related to the free energy,  $F$ , via  $I = -\partial F / \partial \Phi_a$ , where  $\Phi_a$  is the flux through the ring from an applied magnetic field. Measuring  $I$  as a function of  $\Phi_a$  thus tests a fundamental thermodynamic variable and our understanding

of the ring's state. If there are superconducting pairs that are coherent about the ring's circumference  $L$ , the ring's current near zero applied field is proportional to the density of pairs. Deviations from this mean field solution provide information about amplitude and phase fluctuations in the ring.

The mean field G-L solution predicts that the current near zero field should decrease linearly to zero as the temperature,  $T$ , approaches  $T_c$ . For small rings, we find a measurable current above  $T_c$ , a clear signature of fluctuations. The quasi-1D geometry allows a full numeric solution of thermal fluctuations in a G-L framework that includes non-Gaussian effects (5, 6). Previous results on a single ring at zero applied field (7) disagreed strongly with that theory. We studied fluctuations in 15 rings and found that 13 rings agree quantitatively with a full numeric solution, which was numerically intractable for the other 2 rings [Supporting Online Material (SOM) text].

The results in an applied field are particularly interesting. Little and Parks (8) showed experimentally that  $T_c$  varies as a periodic function of  $\Phi_a$ ,  $T_c(\Phi_a)$ . At half-integer multiples of the superconducting flux quantum,  $\Phi_0$ , the energetic cost of maintaining the flux-induced supercurrent can be larger than the condensation energy, destroying superconductivity. Previous results (9–11) indicate qualitatively that fluctuations are especially important in this regime. We find an enhanced response at  $\Phi_a = \Phi_0/2$  that can be quantitatively explained by G-L thermal fluctuations and demonstrate that a single parameter can characterize the Gaussian and non-Gaussian

<sup>1</sup>Department of Applied Physics, Stanford University, Stanford, CA 94305, USA. <sup>2</sup>Department of Physics, University of Colorado Denver, Denver, CO 80204, USA.

\*To whom correspondence should be addressed. E-mail: [kmoler@stanford.edu](mailto:kmoler@stanford.edu)